Nanostructured TiC/a-C coatings for low friction and wear resistant applications

Y.T. Pei[a], D. Galvan[a], J.Th.M. De Hosson[a],*, A. Cavaleiro[b]

[a]Department of Applied Physics, Materials Science Center and Netherlands Institute for Metals Research, University of Groningen,
Nijenborgh 4, 9747 AG Groningen, The Netherlands
[b]Departamento de Engenharia Mecanica, FCTUC-Universidade de Coimbra Pinhal de Marrocos, 3030 Coimbra, Portugal

Abstract

Closed-field unbalanced and balanced magnetron sputtering was used to deposit nanocrystalline TiC (nc-TiC)/amorphous carbon (a-C) nanocomposite coatings with hydrogenated or hydrogen-free a-C matrix, respectively. The contents of Ti and C in the coatings have been varied over the full range of interest (7–45 at.% Ti) by changing the flow rate of acetylene gas or the locations of substrates relative to the center of C/TiC targets. Different levels of bias and deposition pressure were used to control the nanostructure. The nanocomposite coatings exhibit hardness of 5–35 GPa, hardness/E-modulus ratio up to 0.15, wear rate of 4.8×10^{-17} m^3/N m lap, friction coefficient of 0.04 under dry sliding and strong self-lubrication effects. The nanostructure and elemental distribution in the coatings have been characterized with cross-sectional and planar high-resolution transmission electron microscopy (HRTEM) and energy-filtered TEM. The influence of the volume fraction and size distribution of nc-TiC on the coating properties has been examined.
© 2004 Elsevier B.V. All rights reserved.

Keywords: Nanocrystalline TiC; Amorphous carbon; High-resolution transmission electron microscopy; Tribological properties

1. Introduction

Nanocomposite coatings composed of crystalline/amorphous nanophases mixture have recently attracted increasing interests in fundamental research and industrial applications, because of the possibilities of synthesizing a surface protection layer with unique physical–chemical properties that are often not attained in the bulk materials. By controlling the size and volume fraction of nanocrystalline phases in an amorphous matrix and consequently the separation width of amorphous matrix among the nanocrystallites, the properties of the nanocomposite coatings can be tailored, e.g., to make a balance between hardness and elastic modulus to permit close match to the elastic modulus of substrates [1], and particularly to obtain high toughness that is crucial for applications under high loading contact and surface fatigue [2]. In addition to these

characteristics, amorphous carbon (a-C) based nanocomposite coatings exhibit not only excellent wear resistance but also low friction due to self-lubrication effects, which make them environmentally attractive because lubricants can be omitted. This paper focuses on the deposition and characterization of TiC/a-C nanocomposite coatings. Detailed mechanical examinations, including nanoindentations, scratch and tribo-tests, have been performed. Cross-sectional and planar TEM observations and energy-filtered TEM are employed to characterize the nanostructure, elements distribution in the coatings and chemistry of the carbon matrix, respectively. The influence of the volume fraction and size distribution of nanocrystalline TiC (nc-TiC) on the coating properties has been examined.

2. Experimental

Hydrogen-free nc-TiC/a-C nanocomposite coatings were deposited by co-sputtering graphite and TiC targets in a balanced magnetron sputter with a combination of RF and

---

* Corresponding author. Tel.: +31 50 363 4898; fax: +31 50 363 4881.
E-mail address: hossonj@phys.rug.nl (J.T.M. De Hosson).

DC power supply. The initial pressure of the deposition chamber before sputtering was $4–5\times10^{-6}$ mbar and the deposition pressure of argon was 5×10^{-3} or 1×10^{-2} mbar. Hydrogenated nc-TiC/a-C:H coatings were deposited with closed-field unbalanced magnetron sputtering in an argon/acetylene atmosphere in a Hauzer HTC-1000 coating system, which was configured of two Cr targets and two Ti targets opposite to each other. The detailed set-up of the coating system has been documented elsewhere [3]. The Cr targets were used to create an intermediate layer between the nc-TiC/a-C:H coating and the substrate material. The flow rate of acetylene and substrate bias varied in the range of 80–125 sccm and 0–150 V, respectively, to obtain different C/Ti contents and nanostructures in the coatings. The substrates used for each coating were $\oslash 30 \times 5$ mm discs of hardened M2 steel, 304 stainless steel and $\oslash 100$ mm Si wafer for the measurements of residual stress by monitoring the curvature change.

Tribo-tests were performed on a CSM tribometer with a ball-on-disc configuration at 0.1 m/s sliding speed and 2 or 5 N normal load. A CSM Revetest scratch tester was used for measuring the interfacial adhesion strength with a diamond stylus of 200 μm radius and 0.01 m/min scratch speed. A fully calibrated MTS Nano Indenter XP was employed to measure the hardness and Young's modulus of the coatings with a Berkovich indenter and the fracture toughness with a cube-corner indenter according to Lawn–Evans–Marshall's approach [4,5].

The surface morphology and fractured cross sections of the coatings were examined using a scanning electron microscope (SEM; Philips FEG-XL30s). The investigation of the nanostructures was carried out in a high-resolution transmission electron microscope (HRTEM; JEOL 4000 EX/II, operated at 400 kV) and an analytical TEM (JEOL 2010F-FEG, operated at 200 kV). Electron probe microanalysis (EPMA) with a Cameca SX-50 equipment was used to determine the chemical composition of the coatings.

3. Results and discussions

3.1. nc-TiC/a-C nanocomposite coatings

A special configuration of substrates/targets was used to obtain a large composition gradient in a single batch of deposition. As sketched in Fig. 1a, nine pieces of substrates were aligned in a row, from the center of graphite target to the center of TiC target or Ti target, and stayed stationary during deposition of the top coatings. Depending on the relative locations of substrates to the two targets, the composition of deposited coatings may continuously vary from Ti-doped DLC to pure TiC in the case of graphite and TiC targets used, as shown in Fig. 1b. This method allows a
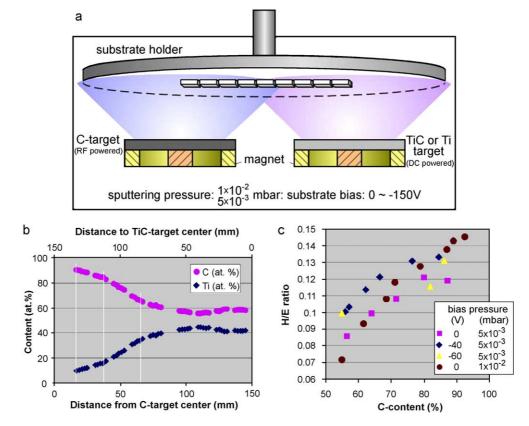

Fig. 1. (a) Sketch of setup for deposition of nc-TiC/a-C coatings; (b) C/Ti content gradient achieved in a batch deposited at −40 V substrate bias and 5×10^{-3} mbar pressure and (c) H/E ratio vs. carbon content under various deposition conditions.

Table 1
Deposition parameters and properties of nc-TiC/a-C coatings deposited with TiC and C targets

Deposition pressure	Substrate bias (V)			
	0	−40	−60	−80[a]
5×10^{-3} mbar	Ti content: 11.9–49 at.%; hardness: 10–16 GPa; *H/E* ratio: 0.121–0.086	Ti content: 10–45 at.%; hardness: 14–27.5 GPa; *H/E* ratio: 0.143–0.100	Ti content: 12–45 at.%; hardness: 20–37 GPa; *H/E* ratio: 0.131–0. 099	Ti content: 12–75 at.%; hardness: 21–35 GPa; *H/E* ratio: 0.117–0.082
1×10^{-2} mbar	Ti content: 6–45 at.%; hardness: 6.9–9.5 GPa; *H/E* ratio: 0.145–0.072	–	Ti content: 8–45 at.%; hardness: 11–14.2 GPa; *H/E* ratio: 0.118–0.080	–

[a] With C and Ti targets.

quick search for the desired composition and associated deposition parameters. Due to the limit of two targets and low sputtering yields of graphite targets, it was rather difficult to optimize the microstructure of both the intermediate layer and the top coating simultaneously. Eventually, a compromise of using TiC and C targets was necessary to obtain the desired C contents in the coatings and the intermediate layer was TiC.

Table 1 summarizes the deposition parameters used and the corresponding coating performances. In general, an increase in substrate bias results in a significant increase in the hardness of nanocomposite coatings. Under the same deposition conditions (i.e., in the same batch), both the hardness and Young's modulus of the coatings increase with Ti content. However, the increasing amplitude of the latter is larger than that of the former, which leads to a decrease in *H/E* ratio with Ti content, as shown in Fig. 1c. Substrate bias and deposition pressure may also have an influence on the *H/E* ratio by altering the intensity of ion bombardment that governs the sizes/distribution of TiC nanocrystallites and the residual stress in the coatings, but not so remarkable as effects exerted onto the individual *H* and *E* parameters.

A high *H/E* ratio is feasible, as shown in Fig. 1c. Although for a long time hardness has been regarded as a primary material property affecting wear resistance, the elastic strain to failure, which is related to the *H/E* ratio, is a more suitable parameter for predicting wear resistance [6]. Within a linear-elastic approach, this is understandable according to the relations that the yield stress of contact is proportional to (H^3/E^2) and the equation $G_c=\pi a\sigma_c^2/E$

indicating that the fracture toughness of coatings defined by so-called 'critical strain energy release rate' G_c would be improved by both a *low* Young's modulus and a *high* critical stress (σ_c) for fracture which implies a need for high hardness.

Associated to the change in properties is the evolution in microstructure of the nanocomposite coatings. SEM micrographs of the fractured cross sections presented in Fig. 2 clearly show the transition from glassy to columnar growth and also enhanced surface roughness of the coatings as Ti content increases. As shall be discussed later, the columnar boundaries are potential weak points of the coatings where growth defects occur and cracks can initiate and propagate through under contact of high loading.

3.2. nc-TiC/a-C:H nanocomposite coatings

The deposition parameters and mechanical properties of nc-TiC/a-C:H nanocomposite coatings are listed in Table 2. Increasing substrate bias leads to an obvious increase in both the hardness and elastic modulus of the nanocomposite coatings. However, the *H/E* ratio stays almost constant when the substrate bias is above 60 V. On the other hand, higher flow rate of acetylene gas, i.e., higher C content results in markedly higher *H/E* ratios, which is analogues to the results in Fig. 1c obtained in the nc-TiC/a-C nanocomposite coatings.

Besides the change from glassy to columnar growth with increasing the Ti content, similar to that observed in nc-TiC/a-C coatings, nc-TiC/a-C:H coatings also exhibit such a
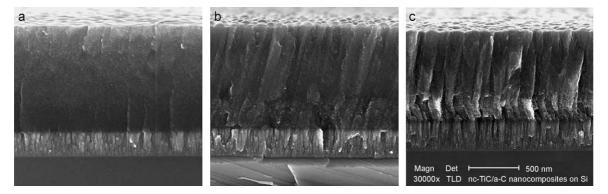

Fig. 2. SEM micrographs of the fractured cross-sections showing the transition from glassy to columnar growth of nc-TiC/a-C coatings with Ti content (at.%) of (a) 10, (b) 17 and (c) 34.

Table 2
Deposition parameters and mechanical properties of nc-TiC/a-C:H nano-composite coatings

Coating no.	C_2H_2 (sccm)	Bias (V)	Stress (MPa)	H (GPa)	E (GPa)	H/E
HB1	110	0	−649	5.5	61.3	0.091
HB2	110	60	−352	11.8	99.8	0.118
HB3	110	100	−761	15.2	136.6	0.111
HB4	110	150	−1595	19.8	168.3	0.118
HB5	80	100	−1184	20.0	229.4	0.087
HB6	125	100	−1154	15.8	128.5	0.123

transition with a decrease in substrate bias, as shown in Fig. 3. The columnar microstructure gets slightly weaker at 60 V bias compared with that at 0 V (floating bias) and is hardly traceable at 100 V so that the fractured cross section looks featureless except for some torn lips. Increasing the substrate bias further to 150 V, the coatings become harder and are fully free of columnar growth and consequently, the fractured cross sections appear flat and show only some contrast of exposed nanoparticles. Cross-sectional TEM observations show a transition of growth mechanism and the columnar structures are restrained at higher substrate bias and C content.

High-resolution TEM presented in Fig. 4 clearly reveals that nanocrystalline TiC particles are homogeneously embedded in the a-C:H matrix and an increase in Ti content leads to the formation of bigger TiC particles, e.g., 2 nm vs. 5 nm in diameter observed in the two coatings consisting of 17.84 and 31.75 at.% Ti, respectively. According to the calculations based on the Ti content of the nanocomposite coatings and a simple model of hard spheres in fcc arrangement, the volume fraction of TiC nanocrystallites in the two coatings are estimated to be 0.31 and 0.59, respectively, with 0.75 nm separation width of a-C:H matrix among TiC nanocrystallites, which is consistent with the HRTEM observations.

Fracture toughness measurements by nanoindentation with a cube-corner tip have recorded a toughness value of 39.97 MPa·m$^{-1/2}$ on the coating HB3 and 33.36 MPa·m$^{-1/2}$ on HB5. SEM observations on indentation impressions demonstrate that the radial cracks propagate readily through the columnar boundaries and leave a meandering crack path in the coating HB5, as seen in Fig. 5b. In contrast, the radial cracks are straight lines in the coating HB3 where columnar structures are restrained. In this sense, one may conclude that an ideal coating should be free of columnar structures.
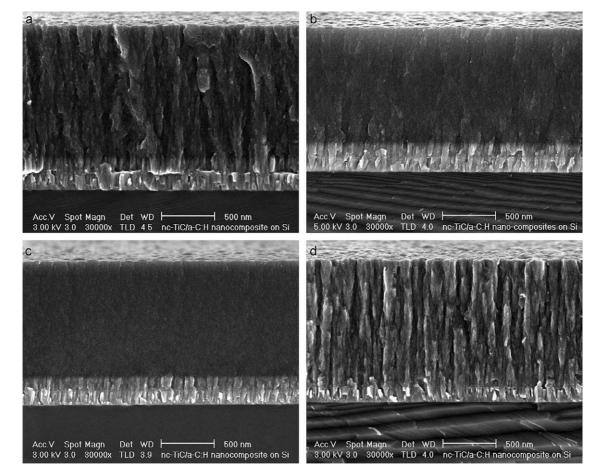

Fig. 3. SEM micrographs of fractured cross-sections showing the transition from columnar to glassy structures of nc-TiC/a-C:H coatings deposited under different conditions: (a) 110 sccm C_2H_2 and −60 V bias; (b) 110 sccm C_2H_2 and −100 V bias; (c) 110 sccm C_2H_2 and −150 V bias and (d) 80 sccm C_2H_2 and −100 V bias.
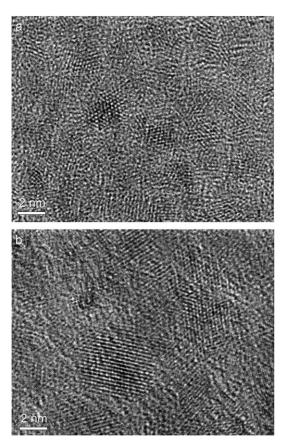
Fig. 4. HRTEM micrographs showing TiC nanocrystallites embedded in a-C:H matrix in nc-TiC/a-C:H nanocomposite: (a) coating HB3 with 17.84 at.% Ti and (b) coating HB5 with 31.75 at.% Ti.
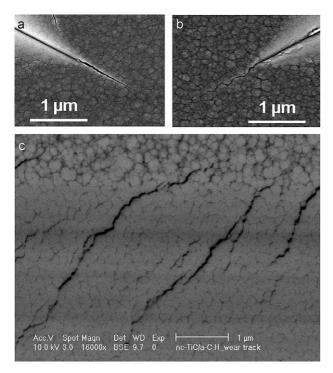

Fig. 5. Radial cracks induced by nanoindentation in the coating HB3 (a) and HB5 (b). (c) Surface fatigue cracks formed in a wear track on the coating HB5.

3.3. Tribological behavior of nanocomposite coatings

Ball-on-disk tribo-tests have been systematically performed on the nanocomposite coatings under loading conditions of maximum 1.5 GPa Hertzian pressure with $\oslash$6 mm balls. The coating HB3 shows the lowest friction coefficient of about 0.04 against 100Cr6 bearing steel balls, as shown in Fig. 6a. The friction coefficient of the coatings HB1 and HB5 is above 0.2, i.e., much higher than that of the coating HB3. Against different counterparts, i.e., alumina balls and bearing steel balls, only slight differences in the friction coefficient are observed in all of the three coatings. The most interesting results are the self-lubrication effects observed on the coating HB3, as seen in Fig. 6b. During the course of transferring films onto the ball surface from the wear track of the coating, the friction coefficient continuously decreases until a stationary state is reached where the lowest level of the coefficient is achieved. To prove this self-lubrication effect, experiments were done in such a way that a fresh surface area of the ball was placed on the same wear track after the stationary state was reached. The friction
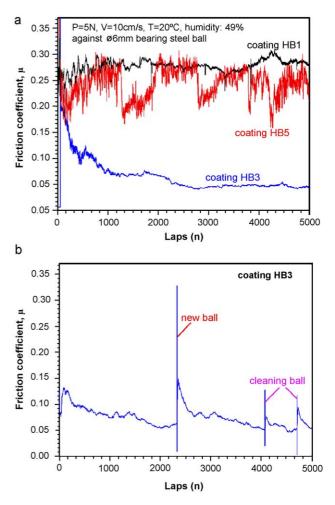

Fig. 6. Tribo-test results showing the friction coefficient of nc-TiC/a-C:H nanocomposite coatings on hardened M2 tool steel substrates: (a) three coatings against bearing steel balls and (b) self-lubrication effects observed on the coating HB3 against bearing steel ball.

coefficient immediately jumped up to a value that characterizes the friction between the fresh steel surface and the coating. Again, the friction coefficient dropped down quickly as the transfer films were gradually covering the ball surface, as seen in Fig. 6b. Further experiments were just to clean the contact area of the ball by rinsing with ethanol and drying with dry N_2, which resulted in small peaks in the graph of friction coefficient followed by a quick drop in friction again. However, the coefficient at these peaks are still lower than that when a fresh surface of the ball was brought into contact with the wear track, possibly attributed to partially adhered films that could not be cleaned completely.

SEM element mapping presented in Fig. 7 shows the transfer films on the contact area of the balls, which supports the self-lubrication mechanism observed. Self-lubrication effects have also been observed on nc-TiC/a-C nanocomposite coatings with glassy growth features, similar to the situation in the nc-TiC/a-C:H nanocomposite coatings. DLC coatings are known for their low friction coefficients due to the hydrophobic nature of DLC surface [7], although the friction behavior of hydrogenated and hydrogen-free DLCs differs in the formation mechanism of transfer films on the contact surface of counterparts: The former makes the contact in-between two basically similar hydrophobic a-C:H surfaces

Table 3
Tribo-test conditions and wear rate of nc-TiC/a-C:H coatings

Coating no.	Ball	Laps	Load (N)	Wear rate ($\times 10^{-15}$ m^3 N^{-1} m^{-1} lap^{-1})
HB1	Al$_2$O$_3$	12 000	2	1.5
	Al$_2$O$_3$	5000	5	3.9
	100Cr6	12 545	2	2.2
	100Cr6	10 630	5	1.4
HB3	Al$_2$O$_3$	25 000	2	0.049
	Al$_2$O$_3$	12 500	2	0.14
	Al$_2$O$_3$	5000	5	0.20
	100Cr6	12 500	2	0.048
	100Cr6	5000	5	0.089
HB5	Al$_2$O$_3$	12 500	2	2.8
	Al$_2$O$_3$	5000	5	1.5
	100Cr6	12 500	2	3.1
	100Cr6	5000	5	1.8

and in the latter a graphitic layer acts as solid lubricant. The friction behavior of nc-TiC/a-C(:H) nanocomposite coatings is more complicated compared with pure DLCs. If the a-C(:H) matrix cannot efficiently shield TiC particles in the transfer films as in the cases of nanocomposite coatings with a high volumetric fraction of (rather big) TiC nanocrystallites, TiC nanoparticles may cause lots of damages to the hydrophobic contact surfaces or to the graphitic layer formed. This may explain the fluctuations in the friction graph of HB5, as shown in Fig. 6a.

Efforts were made to measure the wear rate of different coatings after tribo-tests. With a confocal microscope, eight images of 3D profiles were captured at different positions on a wear track for reliable average. A software code in MatLab was then used to calculate the volumetric loss (V) of a wear track and finally the wear rate (W_r) of the coatings defined as volume of wear per unit track length, per Newton of normal load and per lap. The wear rate of different coatings is summarized in Table 3. The coating HB3 of high H/E ratio above 0.1 exhibits a wear rate as low as 4.8×10^{-17} m^3/N m lap against bearing steel ball. It is expected that the wear rate may decrease further as more laps are run in a tribo-test. SEM observation of the wear tracks shows that surface fatigue cracks initiate at and propagate through the columnar boundaries under ball contact, as shown in Fig. 5c. No cracks are observed in the wear tracks on the coating HB3 where columnar structures are restrained.

4. Conclusions

The nc-TiC/a-C(:H) nanocomposite coatings have been successfully deposited by magnetron sputtering, which consist of TiC nanocrystallites embedded in amorphous carbon matrix. Small TiC particle size (2 nm) and low volumetric fraction (~0.3) result in very homogeneous micro/nanostructures of the nanocomposite coatings that combine low friction with high toughness and wear
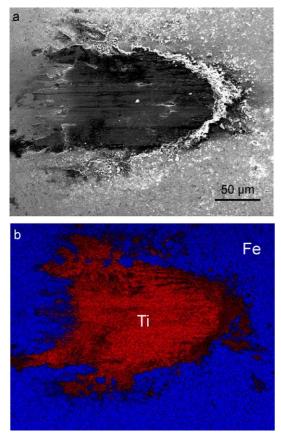
Fig. 7. SEM elements mapping reveals transfer films on the contact area of steel ball from nc-TiC/a-C:H coatings: (a) SEM micrograph of the contact area and (b) Ti and Fe element mapping.

resistance. The columnar structure varies as a function of Ti content and substrate bias, and can be restrained to achieve supertoughness in these nanocomposite coatings. The H/E ratio is mainly dominated by C content and reaches high values above 0.1 at high C contents, which result in high wear resistance. Self-lubrication can be achieved at high volumetric fraction of amorphous carbon matrix together with homogeneously distributed TiC nanocrystallites.

Acknowledgments

References

[1] W.J. Meng, B.A. Gillispie, J. Appl. Phys. 84 (1998) 4314.
[2] A.A. Voevodin, J.S. Zabinski, Thin Solid Films 370 (2000) 223.
[3] C. Strondl, N.M. Carvalho, J.Th.M. De Hosson, G.J. van der Kolk, Surf. Coat. Technol. 162 (2003) 288.
[4] G.M. Phar, Mater. Sci. Eng., A Struct. Mater.: Prop. Microstruct. Process. 253 (1998) 151.
[5] B.R. Lawn, A.G. Evans, D.B. Marshall, J. Am. Ceram. Soc. 63 (1980) 574.
[6] A. Leyland, A. Matthews, Wear 26 (2000) 1.
[7] J. Robertson, Mater. Sci. Eng., R Rep. 37 (2002) 129.